Journal of Alloys and Compounds 523 (2012) 167–175

Contents lists available at SciVerse ScienceDirect

Journal of Alloys and Compounds

journal homepage: www.elsevier.com/locate/jallcom

Alloying and microstructural changes in platinum–titanium milled and annealed powders

Kasonde Maweja [a,b,*], M.J. Phasha [a], Y. Yamabe-Mitarai [c]

[a] The Council for Scientific and Industrial Research, CSIR, Metals and Metals Processes, Lynnwood Manor, P.O. Box 395, Pretoria 0001, South Africa
[b] Element Six Production Ltd, Diamond Research Laboratory, 1 Debid road, Nuffield, PO Box 561, Springs 1559, South Africa
[c] National Institute of Materials Science, NIMS, Sengen 1-2-1, Tsukuba, Ibaraki 305-0047, Japan

ARTICLE INFO

Article history:
Received 13 July 2011
Received in revised form 25 January 2012
Accepted 27 January 2012
Available online 7 February 2012

Keywords:
Ti–Pt
Mechanical alloying
Ball milling
Annealing
Martensite

ABSTRACT

Equiatomic platinum–titanium powder mixtures were processed by high energy ball milling under argon atmosphere and sintered under vacuum. Evolution of the crystal structures and microstructures of the products formed were investigated by XRD and SEM techniques, respectively. The HCP crystals of Ti were first deformed and then a disordered metastable FCC Pt(Ti) solid solution was formed during milling due to semi-coherency of FCC lattices. A nanostructured Pt(Ti) product was formed after long milling time, which contained 44–47 at.% Ti and 53–56 at.% Pt.

An ordered PtTi intermetallic was formed by annealing the metastable Pt(Ti) at temperature above 1300 °C. The crystal structure and microstructure of the TiPt phase depended on the milling time, annealing temperature and the cooling rate. The B19 PtTi plate martensite was formed after annealing at 1500 °C and quenching at a cooling rate of 23 °C/min to 200 °C/min for short time milled products. The width of martensite features was smaller at high cooling rate. In PtTi products milled for longer time, no martensitic transformation was observed on cooling the annealed samples. Small amounts of Pt_5Ti_3 were formed in the powders milled for 16 h or more, followed by annealing at 1500 °C and furnace cooling at ~2 °C/min.

1. Introduction

NiTi alloys are commonly developed for use as shape memory alloys. However, the maximum temperature they can be used at is about 100 °C, due to the limitations of available transformation temperatures. The PtTi phase in cast alloys has been recognised for its potential as a shape memory alloy because of its martensitic transformation from high temperature body centred cubic B2 to orthorhombic B19 at ~1000 °C [1–5]. The reported corresponding transformation temperatures are below the solid parabolic line in Fig. 1.

The martensitic phase transformation temperature of NiTi-based alloys, which is related to the shape memory effect, was increased above 100 °C by partial or total substitution of Ni by some precious metals such as platinum, palladium, ruthenium and gold [6–19]. The PdTi compound was considered as a very good candidate since the intermetallic PdTi undergoes a thermoelastic transformation around 530 °C [19] but the recrystallisation process in the martensitic state alters the shape memory effect [6]. The shape memory characteristics were improved by precipitation hardening at 500 °C or by thermomechanical treatment. The improvement was attributed to the increase in critical stress for slip in the parent phase (B2) [9]. The AuTi alloy has also received a large interest, and a one-way shape memory effect has been reported qualitatively [15–19].

Pseudo-elastic behaviour and 10% strain recovery were found in Ti–Pt–(Ir, Ru) arc melted alloys with different heat treatments below the phase transformation temperature (~900 °C) [4,5]. Potential limitations in expected strain recovery were attributed to inhomogeneous microstructures of Pt–Ti based alloys produced by arc melting [4]. High-energy ball milling may be a simple and practical route for the synthesis of nanostructured products with improved homogeneity [20–22].

Substantial studies have been reported on the development of porous and dense NiTi-based alloys with shape memory effects by the powder metallurgy route [23–38]. Based on these studies, it was established that milling time affected the porosity of sintered products [23] and that the formation of additional phases and Kirkendall porosity was difficult to avoid when elemental powders were chosen as starting materials [35,36].

Abbasi and Shamanian [39,40] reported the formation of intermetallics during annealing of short time milled products whereas formation of nanostructured composites was favoured in annealing of products milled for longer periods. Martensitic transformation

* Corresponding author. Tel.: +27 83 365 0952.
E-mail address: mawejak@yahoo.fr (K. Maweja).

0925-8388/$ – see front matter © 2012 Elsevier B.V. All rights reserved.
doi:10.1016/j.jallcom.2012.01.149

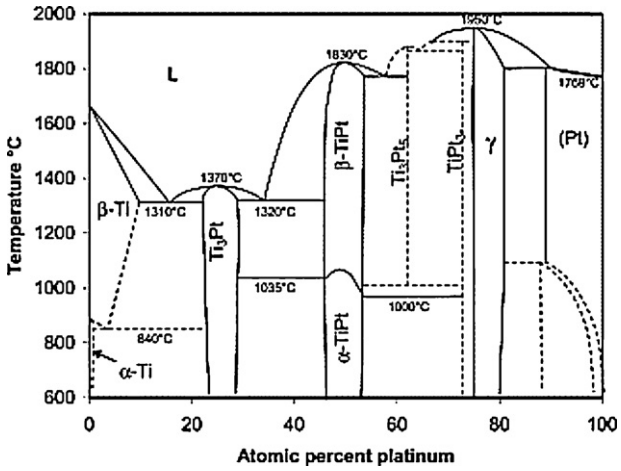

Fig. 1. Ti–Pt equilibrium phase diagram [3].

in NiTi shape memory alloys prepared by the powder metallurgy route was affected by the milling conditions. Tian et al. [41] observed that crystallized powders exhibited martensitic transformation with reduced heat effect. The critical temperatures for the transformations were found to decrease with increasing ball milling time. A suppression of martensitic transformation in the annealed powders could be related to the grain refinement of the austenite phase in the powder particles [42]. Investigation by Valeanu et al. [43] on the martensitic transformation in Ti–Ni–Cu alloys reported the transformation sequence B2-B19-B19′ observed in alloys prepared by melting route was no longer valid for the alloys prepared by mixing in a high energy ball mill. Instead, two independent martensitic transformations, B2-B19 and B2-B19′, took place. Furthermore, according to the same study, a longer milling process promoted the formation of a non-transforming phase [43].

Most reported investigations on the binary Pt–Ti and ternary Pt–X–Ti alloys were produced by arc melting. The present work investigated the microstructural evolution and alloying mechanisms in elemental Pt–Ti powder mixtures processed by high energy ball milling and subsequent heat treatment. The effects of milling time, annealing temperature and cooling rate on the phase formations were analysed.

2. Experimental procedure

Equiatomic mixtures of elemental Pt (99.5% purity, 100–200 μm) and Ti (99.5% purity, particle size < 45 μm) powders were processed by high energy ball milling. Stearic acid (2.5 wt% of powder total mass) was added as a process control agent. The mixtures were milled in an argon atmosphere using a Simoloyer CM01 machine for times varying between 1 and 32 h. Milling media consisted of 5 mm diameter 3Cr12 stainless steel balls. In order to minimize contamination of the milled powder by the milling media, an amount of Ti powder was first milled for 8 h to form a protecting layer on the surface of the balls and the milling jar. A ball-to-powder mass ratio of 20:1, and a rotation speed of 800 rpm were employed. The ball milling induced changes in powders were analysed by X-ray diffraction, SEM and TEM techniques.

The powder samples were analysed in a Philips X'Pert powder diffractometer with Ni filtered Cu-Kα radiation. The grain sizes (L) and lattice strains (e) were determined by means of the modified Williamson-Hall method [44] described by equation (1).

$$\delta(2\theta) = \frac{\lambda}{L} + 4e\sin\theta \quad (1)$$

where θ and $\delta(2\theta)$ are the diffraction angle and the corresponding full width at half maximum (FWHM) of the peak, and λ is the X-ray wavelength. The crystal structures of compounds were identified using the ICSD database [45].

The phase distribution inside the particles of the milled powders and their respective compositions were analysed in an ESEM-FEG XL30 Philips instrument

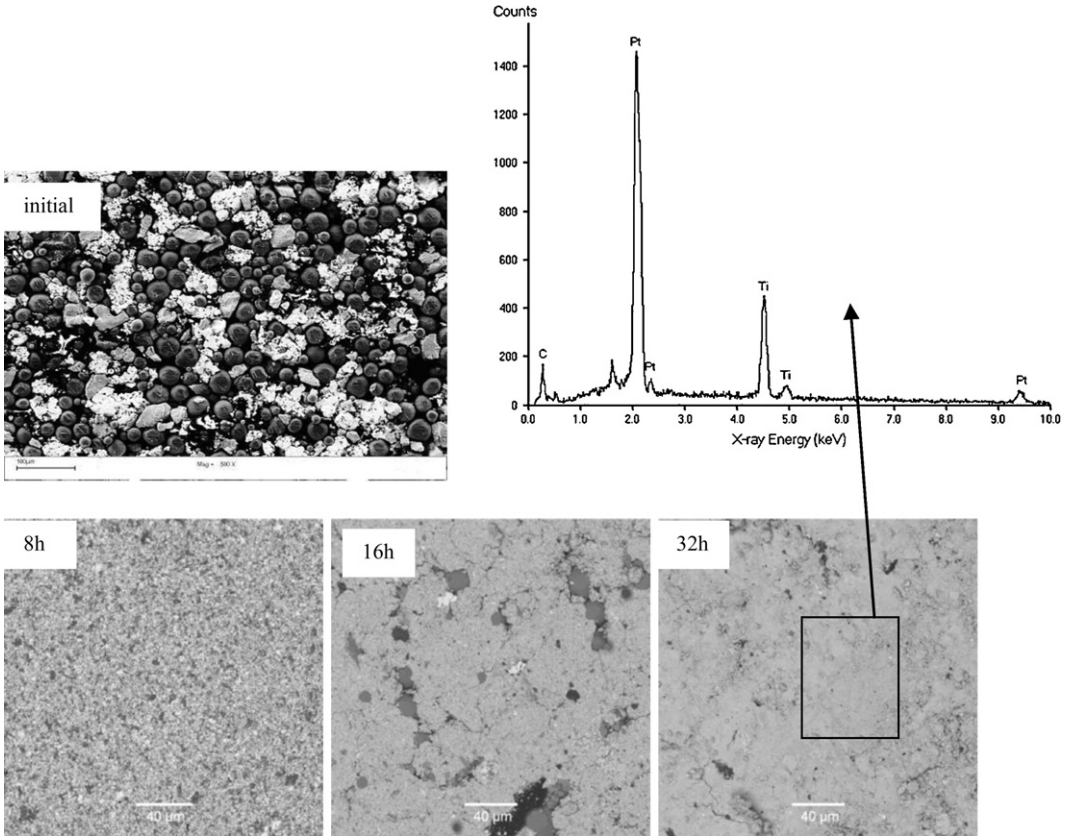

Fig. 2. BSE-SEM micrograph showing a heterogeneous mixture of Pt particles (bright contrast) and Ti particles (dark) in the initial mixture and the effect of milling on the composition of the particles.

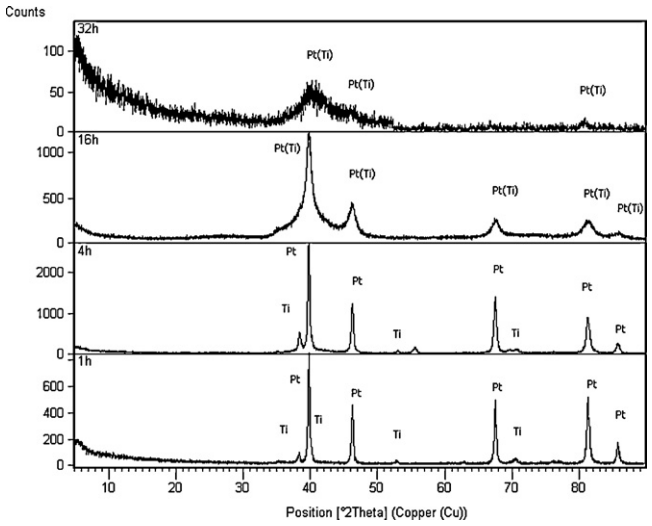

Fig. 3. XRD patterns of the equimolar Pt–Ti mixtures at different milling time showing the decrease in intensities, broadening of the peaks and the slight shift toward higher angles of Pt(Ti) peaks.

equipped with an EDX detector. The powder samples for SEM analysis were mounted on cold resin, grinded on successive grit papers and polished with diamond paste to 1 μm finish. This procedure made it possible to analyse the microstructure inside the cross sections of the powder particles.

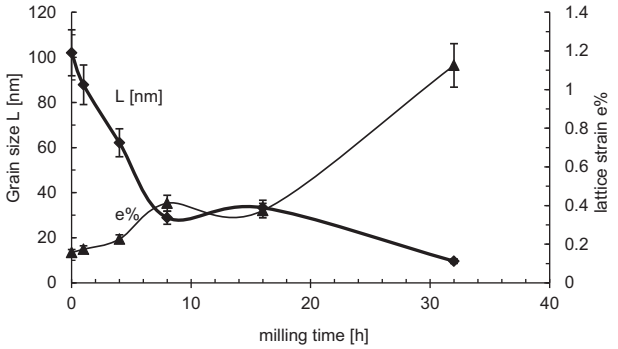

Fig. 4. Grain sizes (filled circles) and lattice strains (filled triangles) of Pt and Pt(Ti) formed by milling elemental powder mixtures.

The transformation temperatures of milled powders were determined by differential thermal analysis at a 10 °C/min heating rate and cooling in DTA-TGA equipment in an argon atmosphere. The milled powders were then compacted at room temperature under 40 MPa in a uniaxial press to form green compact rods. The rods were annealed under 10^{-7} bar vacuum at different temperatures; i.e. 1300 °C, 1400 °C, 1500 °C and 1600 °C, which were lower than the melting temperatures of pure Ti (1650 °C), Pt (1768 °C) and the PtTi alloy (1830 °C). The cooling rate was varied from 2 °C/min (furnace cool) to 23 °C/min and to 200 °C/min in argon gas flow. SEM and XRD analyses were carried out through the cross sections of the heat treated powder particles to characterise the phases formed.

Stearic acid added into the powder mixtures formed a layer around the milling balls and on the inner surfaces of the pots. Another proportion formed thin layers around each particle, which prevented cold welding. The thickness of acid layers

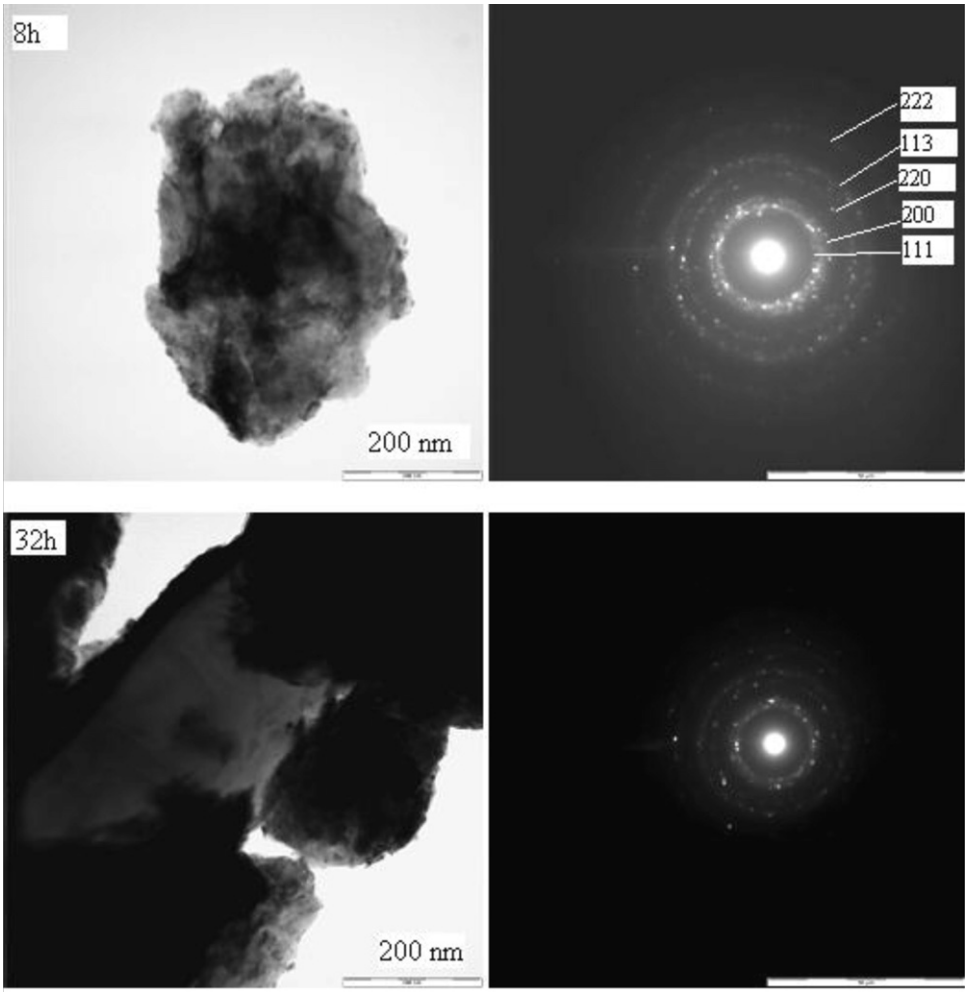

Fig. 5. TEM-BF images and corresponding electron diffraction patterns of powders milled for 8 h and 32 h.

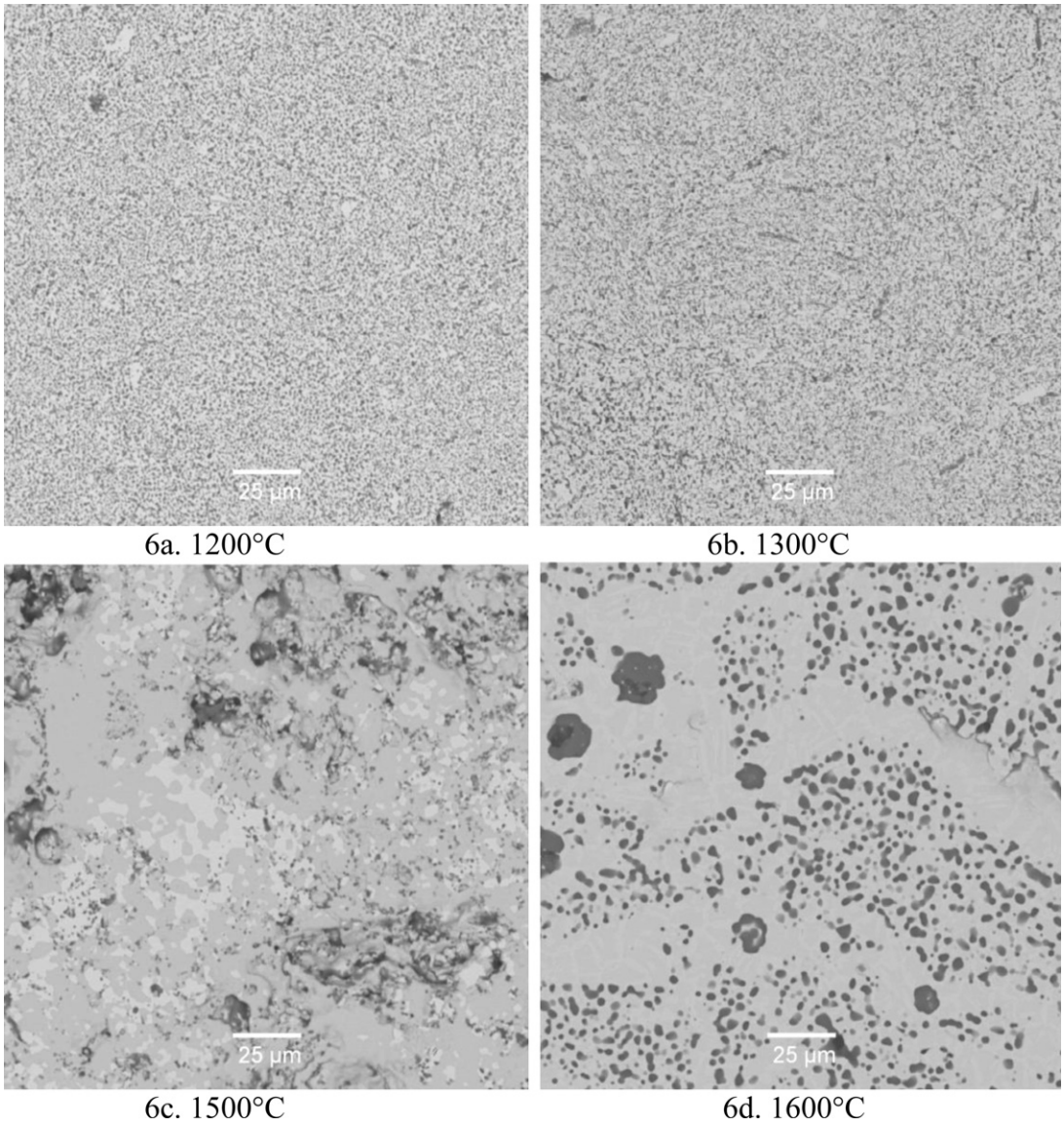

Fig. 6. BSE-SEM micrographs of Pt–Ti mixtures milled for 32 h and annealed at different temperatures.

formed is negligible comparative to the cross sections of the powder particles. The contribution of carbon and oxygen from the stearic acid to the chemical compositions of the cross sections of the milled particles determined by EDX method are therefore negligible. Stearic acid is afterward decomposed into gases during annealing under vacuum.

3. Results and discussion

3.1. Microstructural changes induced by high-energy ball milling

The homogeneity of Pt:Ti powder mixtures was improved by ball milling as shown in Fig. 2. The powder particles were deformed and crushed at the early milling stages. The BSE-SEM images and EDX analysis showed the presence of a main Pt-rich phase (bright contrast) and a small number of Ti-rich particles (dark contrast) in powder mixtures milled for 16 h. The products were more homogenised after 32 h milling. The existence of a small proportion of the Ti-rich phase in the milled products indicated that the harder Ti particles were either dissolved or dispersed into the more ductile Pt particles. The proportion of the Ti-rich particles decreased to ~3 vol.% after milling for 32 h. In order to confirm that mechanical alloying proceeds by dissolution of Ti atoms in the Pt lattices; a mechanism was assessed by X-ray diffraction and TEM analyses of the milled products. The chemical composition determined by EDX analysis of the matrix phase formed after 32 h milling was 53–57 at.% Pt and 43–47 at.% Ti, while the carbon and oxygen contents remained lower than 2 at.%. The two interstitial elements might result from contamination by stearic acid or by gases dissolved during milling.

As shown by XRD patterns in Fig. 3, it was observed that the Pt and Ti peaks became broader and their intensities decreased as milling time increased due to the straining of the lattices and the refinement of the grains. Titanium peaks vanished after 16 h milling, whereas the Pt peaks slightly shifted toward higher 2θ angles. The disappearance of Ti peaks was attributed to the HCP-FCC allotropic transformation [46]. The FCC lattices formed a semi- or coherent interface with FCC Pt crystal lattices, hence leading to the formation of a disordered metastable FCC Pt(Ti) solid solution during ball milling.

The atomic mismatch between Pt (atom radius = 0.183 nm) and Ti (r = 0.200 nm) is 8.5%, which is smaller than 15%. However, even though the oxidation states of the two elements are almost similar, their crystal structures are different. The FCC Pt(Ti) solid solution that is formed at room temperature is disordered and metastable,

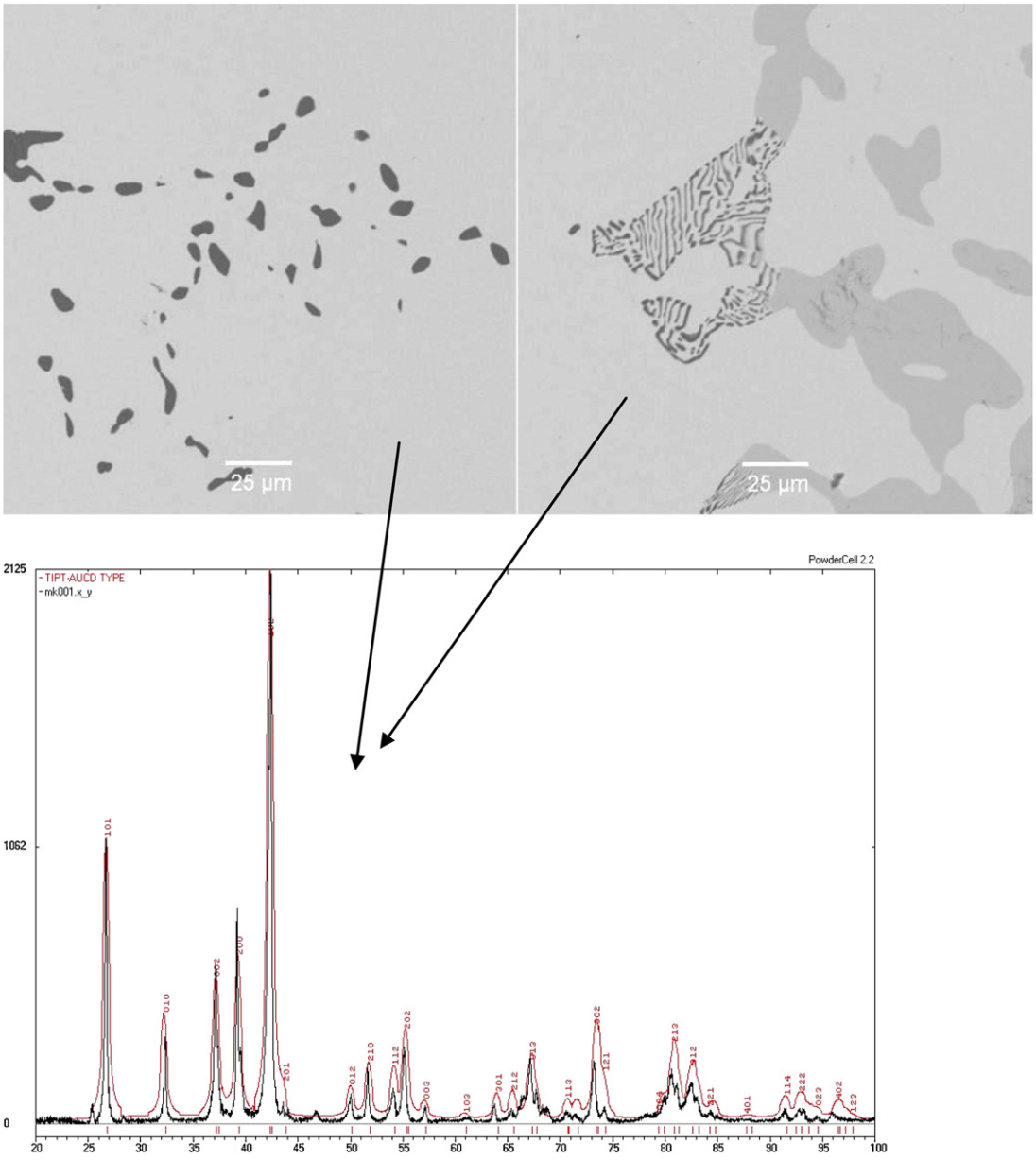

Fig. 7. Typical BSE-SEM micrograph of powder milled for more than 8 h, annealed under vacuum at 1500 °C and cooled at 2 °C/min showing α-$Pt_{53}Ti_{47}$ (light matrix), $PtTi_3$ (grey contrast) and Ti-rich (dark contrast) phases. The corresponding X-ray diffractogram (black line) as well as the calculated diffractogram using Powdercell (red line) are also shown. (For interpretation of the references to color in this figure legend, the reader is referred to the web version of the article.)

in accordance with Hume-Rothery rules of solid-solutions [47]. The α-TiPt is the stable phase at room temperature according to the equilibrium phase diagram. The intensities of the peaks of the Pt(Ti) phase formed became smaller after 32 h milling due to refinement of the grains and the increased lattice strains.

The disappearance of Ti peaks from the X-ray diffraction patterns of powders milled for 16 h also coincides with the formation of a more homogeneous matrix as illustrated in the SEM micrograph in Fig. 2. The shrinkage of Pt(Ti) lattices evidenced by the slight shift of the X-ray diffraction peaks toward the higher angles is brought by shrinkage of FCC Ti lattice in contact with slightly smaller lattice of Pt as a result of a decrease in the *d*-spacing of the platinum crystals.

The grain sizes and lattice strains of Pt and Pt(Ti), formed during mechanical milling, are represented in Fig. 4. The lattice strain of Pt increased to the local maximum of about 0.4 after 8 h milling, before decreasing slightly after 16 h, which corresponded to the vanishing of Ti peaks from the X-ray diffraction patterns. The local maximum also corresponded to the start of the Pt(Ti) solid solution formation. Therefore, the driving force for mechanical alloying during ball milling was attributed in part to the relaxation of the lattice strain in the platinum grains. The lattice strains of Pt(Ti) grains increased faster thereafter reaching a maximum of 1.1 after 32 h milling., whereas the corresponding grain sizes became smaller (∼10 nm). The increase in dislocation density upon milling led to a smaller effective grain size determined by X-ray diffraction method. The XRD peaks of the products milled for 32 h were subsequently broad and had lower intensities.

The FCC crystal structures of the milled products were confirmed by means of electron diffraction method as illustrated in Fig. 5. The camera constant *K* of the TEM machine used was 100 mm. The interplanar distances were determined by the classic $d = K/r$ relationship, where *r* is the distance from the origin in the reciprocal space. The lattice parameter of FCC Pt(Ti) were found to be

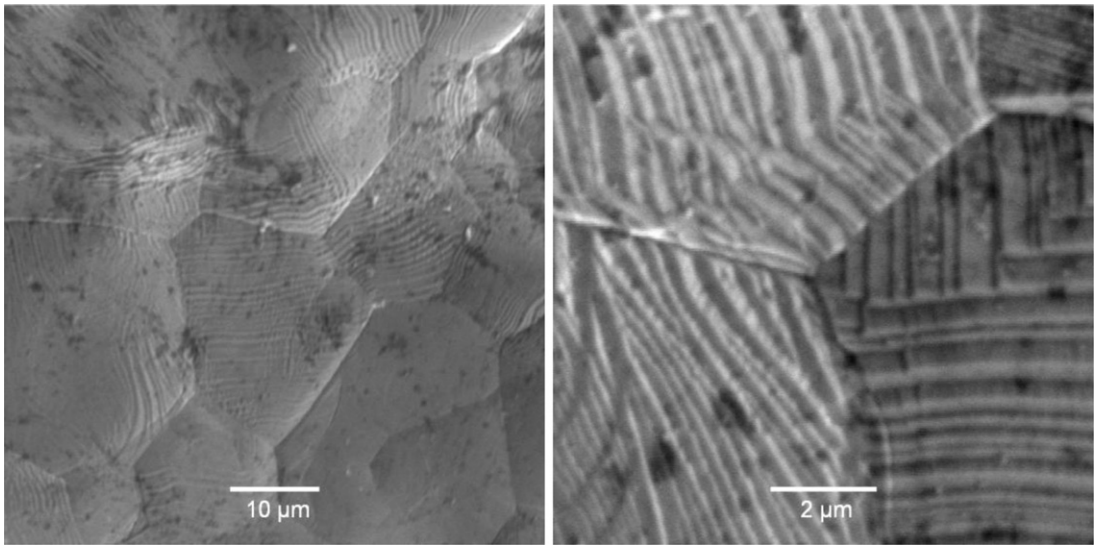

Fig. 8. SE-SEM micrograhs of powders milled for 4 h annealed at 1500 °C and quenched in helium gas flow showing (a) polygonal grains formed and (b) plate martensite formed inside the grains.

0.412 ± 0.010 nm, thus the FCC Pt(Ti) cells expended by ~5% due to substitution of Pt by larger Ti atoms in powders processed by high energy ball milling.

3.2. Annealing behaviour of milled powders

The sintering mechanism of mechanically alloyed Pt(Ti) powders introduced complexities as the annealing temperature and cooling rates affected the microstructures of heat treated products. A product matrix of composition $Pt_{56}Ti_{44}$ (bright contrast) containing a dispersion of fine Ti-rich particles (dark contrast) was formed after annealing at 1300 °C and furnace cooling at 2 °C/min of the powders milled for 32 h (Fig. 6a). The size of the titanium-rich particles increased to ~300 nm after annealing at 1400 °C and cooling to room temperature at the same rate (Fig. 6b). The growth of Ti-rich particles was attributed to a thermally induced decomposition of the metastable Pt(Ti) solid solution formed during milling. These particles coalesced leaving large pores in materials that were annealed at 1500 °C and 1600 °C (Fig. 6c and d).

The coalescence of pores during annealing under vacuum and the contiguity in the matrix are characteristic of formation of a liquid phase at ~1500 °C (Fig. 6c and d), which is lower than the melting temperature of PtTi (1830 °C). Goh et al. [25] have similarly demonstrated the efficiency of using mechanically milled nanocrystalline NiTi as reaction agent in sintering of Ni–Ti powders. They showed that activation barriers for combustion synthesis reaction as well as the portion of unreacted Ni in the final products were lowered.

Annealing the powders milled longer than 8 h at 1500 °C enabled the formation of an ordered $Pt_{53}Ti_{47}$ solid solution matrix phase, which contained $PtTi_3$ particles (grey) in some areas as shown in Fig. 7. A perfect match was found by fitting of the X-ray diffraction data of the material annealed at temperature above 1500 °C with the profile of α-PtTi calculated using Powdercell software [48]. It was difficult to accurately analyse the small phases without collecting X-rays from the adjacent areas.

It was noticed that the matrix phase had higher Pt content than the starting equiatomic powder mixtures. Additionally, the dark Ti-rich regions had a eutectic phase structure. It was therefore attributed to the partial decomposition of the annealed product during the cooling down as indicated in the equilibrium phase diagram.

3.3. Martensite formation in Pt(Ti) milled powders

Martensite surface reliefs were observed in samples of powder mixtures milled for short times (~4 h) that were annealed at temperature between 1500 °C and 1600 °C and cooled at 23 °C/min or 200 °C/min as illustrated in Fig. 8. The width of the martensite features formed varied between 200 nm and 500 nm. The edges of the martensite features lied on the boundaries of the polygonal grains, which indicated the formation of martensite by heterogeneous nucleation on grain boundaries.

The martensite microstructure was also observed in grains of samples milled for 8 h, sintered at 1500 °C and cooled at 2 °C/min as shown in Fig. 9. However, in this case the width of martensite features was much larger, varying from 2000 nm to 8000 nm. Thus, the widths of PtTi martensite features (laths or plates) were smaller at fast cooling rate.

Monastyrsky et al. [24] have also reported the formation of a martensitic β-phase along with other intermediate phases in sintering of Ni–Ti–Zr blended powders and slow cooling to room temperature. According to their work it was noticed that martensite was formed in larger grains when the cooling was slow. This might explain the limited number of twinning planes as observed in Figs. 8 and 9.

The peak identification from the XRD patterns of the powders milled for 4 h annealed at temperature >1500 °C and quenched shown in Fig. 10(a), indicated that the products consisted of orthorhombic B19 PtTi (plate martensite). The small peaks observed at diffraction angles $2\theta = (25.5°, 44°, 47°$ and $78.5°)$ are ascribed to the formation of hexagonal Pt_3Ti_5, which is more distinct in Fig. 10(b) for sample milled for 16 h. The refinement of PtTi XRD data in Fig. 10(a) using the Rietveld method suggested the lattice parameters were $a = 0.48093$ nm, $b = 0.456106$ nm, $c = 0.274378$ nm, $\alpha = 90°$, $\beta = 90°$, $\gamma = 90°$. Similar results were obtained with a cooling rate of 23 °C/min as shown in Table 1.

Table 1
Crystal structures and calculated lattice parameters by Rietveld refinement of X-ray diffraction data of the powder milled for 4 h, annealed and cooled at 23 °C/min.

Structure	a [Å]	b[Å]	c[Å]	$\alpha°$	$\beta°$	$\gamma°$	V
B19	4.5900	2.7618	4.8306	90	90	90	61.24

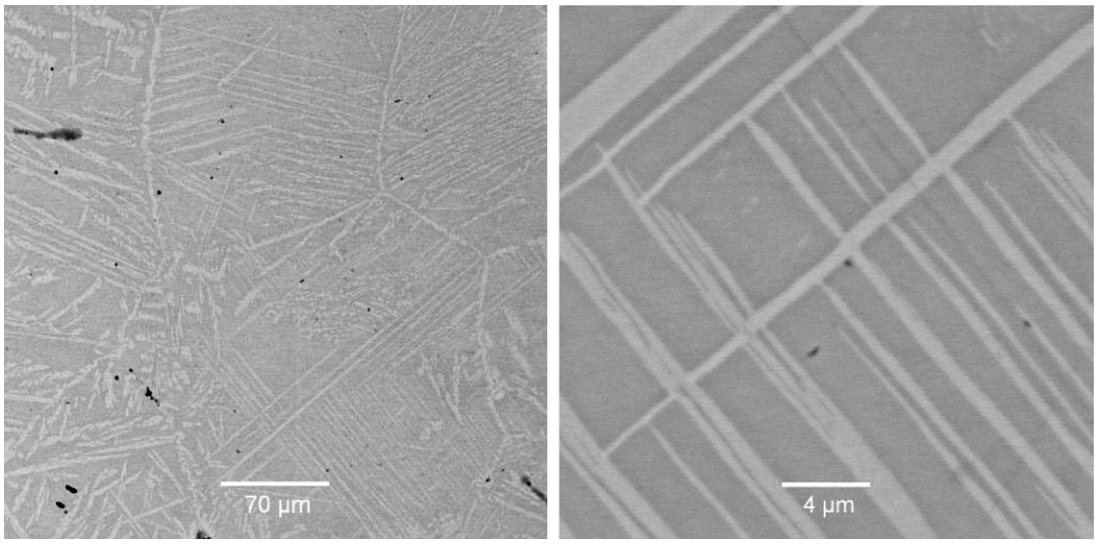

Fig. 9. BSE-SEM micrograph of polished sample of the Ti–Pt powder milled for 8 h, annealed at 1500 °C and cooled by 2 °C/min showing the formation of the martensite plates along well defined planes.

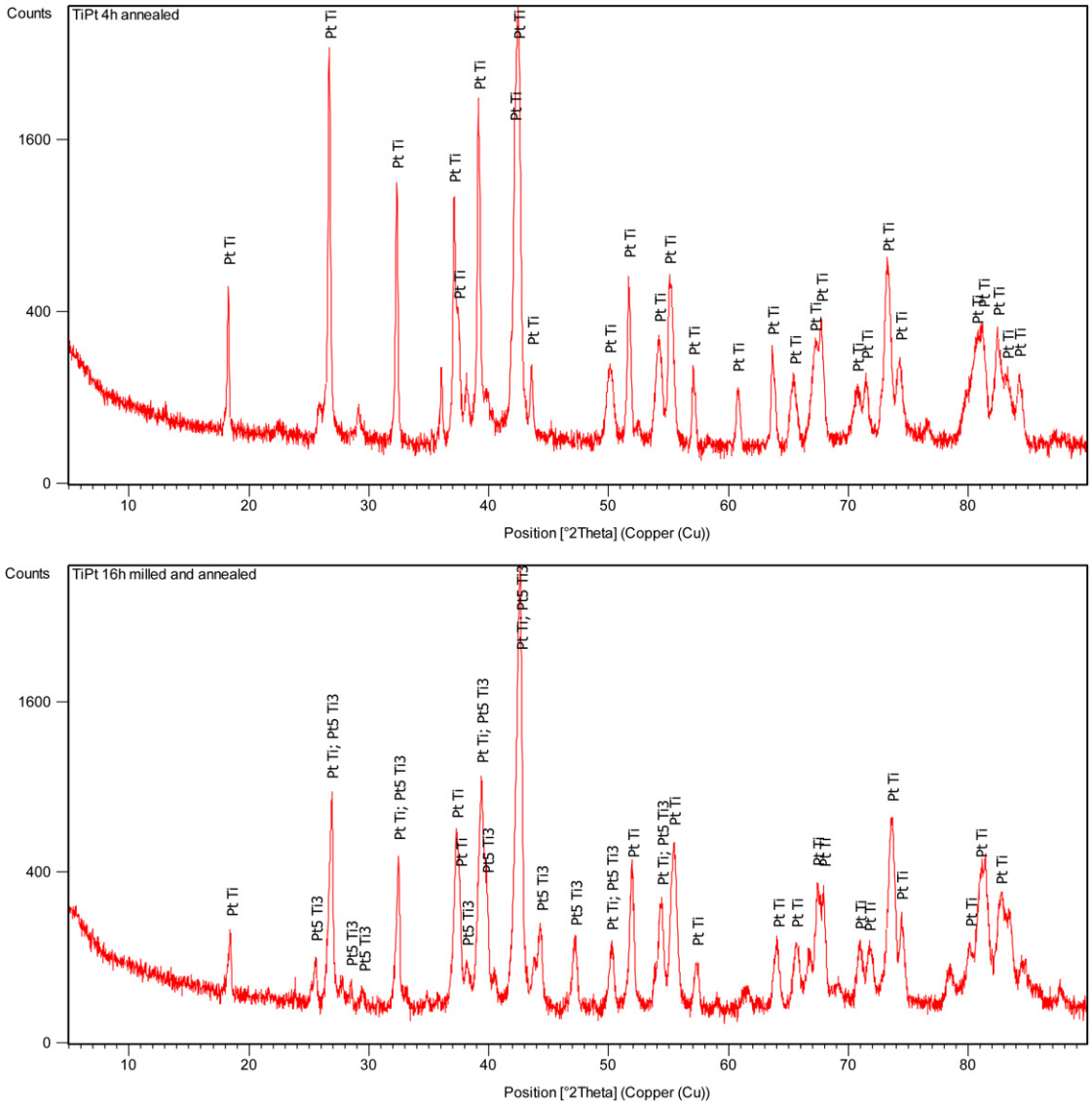

Fig. 10. X-ray diffraction pattern of the sample milled for (a) 4 h and (b)16 h, annealed and quenched at 200 °C/min showing the characteristic peaks of B19 PtTi.

Table 2
DTA cooling transformation temperatures and temperature changes of Pt–Ti powders processed by high energy ball milling.

Milling time	Transformation temperature [°C]		Temperature change ΔT[°C]	
	M1	M2	M1	M2
1 h	740	612	6.1	5.7
4 h	729	595	3.0	2.9
8 h	726	585	2.7	2.8

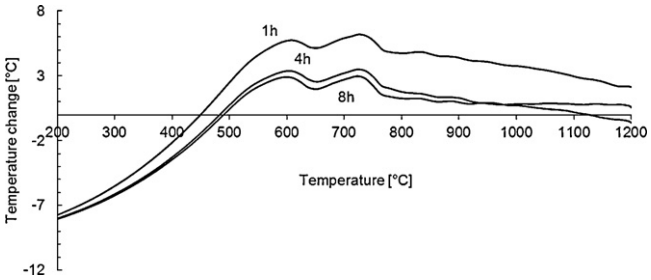

Fig. 11. DTA cooling curves illustrating the effect of the milling time on the transformation temperatures and on the temperature change.

The DTA cooling curves (Fig. 11) of milled powders presented two peaks that shifted to lower transformation temperatures as milling time increased. This variation of transformation temperatures showed that the mechanical energy stored in the strained powder particles, the defects such dislocations and sub-grain structures induced by high energy ball milling contribute to lower transformation temperatures from the higher temperatures reported for PtTi arc melt alloy. The DTA measurements also showed that the magnitudes of the temperature changes during cooling were smaller for powders milled for longer times. Thus the effect of the thermally induced transformations was minimal in products of the longer milling times. The decrease of the magnitudes of temperature change was therefore attributed to formation of a non-transforming PtTi phase. Valeanu et al. [43] reported similar effect of milling time in Ti–Ni–Cu mechanically alloyed powders, where martensitic transformation was suppressed after long treatment by high energy ball milling.

The double peaks observed in the DTA cooling curves indicate two transformations taking place at different temperatures (Table 2), which may be attributed to a martensite transformation: B2 → B19 in particles of different grain sizes experiencing different stains due to inhomogeneity of milling process. Valeanu et al. [43] have recently indicated that in Ti–Ni–Cu processed by high energy ball milled two martensite transformations B2 → B19 and B2 → B19′ occurred independently. The martensite transformation temperatures of Pt–Ti mechanically alloyed powders would therefore be as indicated in Table 2. The transformation temperatures are lower than reported in equilibrium phase diagrams for arc melt PtTi alloy, which transforms at temperatures varying between 900 and 1000 °C [1–3]. Thus, high energy ball milling decreases the cooling down transformation temperatures. A consequence of mechanical alloying will therefore be an increased barrier to martensitic transformation.

4. Conclusion

Equiatomic Pt:Ti mixtures of elemental powders were processed by high-energy ball milling. A disordered metastable FCC Pt(Ti) solid solution was formed. The composition of the product was close to 44–47 at.% Ti and 53–56 at.% Pt, which could contain fine dispersed Ti-rich particles.

The HCP crystals of Ti was first deformed, which led to FCC transition, and then the FCC lattice formed a semi- or coherent interface with FCC Pt lattice, hence leading to the formation of a disordered metastable FCC Pt(Ti) solid solution. The crystals of metastable Pt(Ti) solid solution were then refined and a nanostructured product was formed after 32 h milling.

Fine pores were observed in the Pt(Ti) matrix of products milled for long periods and annealed at 1300 °C. The pores coalesced at higher temperature.

A stable α-TiPt phase was formed after high temperature annealing of powders milled for long times. Martenstic transformation was not observed in these phases, whereas B19 plate martensite phase was formed in products milled for shorter times upon annealing and either quenching or cooling to room temperature.

Rietveld refinement of the XRD data suggested the existence of B19 (orthorhombic), but small signals of hexagonal Pt_3Ti_5 were observed in the product of short time milled powders which were quenched at an intermediate rate (~23 °C/min). The width of the martensite features formed was smaller at higher cooling rates. The presence of Pt_3Ti_5 phase was evident in powders milled for longer than 8 h and subsequent heat treatments. Although homogeneity was improved in powders milled for longer times, one of the consequences is that it also make it easy for formation of other high temperature intermetallic phases, which in turn causes the chemical composition to deviate from that bearing the martensitic transformation.

References

[1] T. Biggs, M.J. Witcomb, L.A. Cornish, Mater. Sci. Eng. A 273–275 (1999) 204–207.
[2] T. Biggs, L.A. Cornish, M.J. Witcomb, M.B. Cortie, J. Alloys Compd. 375 (2004) 120–127.
[3] T.B. Massalski, Binary Phase Diagrams, AMS, USA, 1990.
[4] Y. Yamabe-Mitarai, T. Hara, S. Miura, H. Hosoda, Mater. Trans. 47 (3) (2006) 650–657.
[5] Y. Yamabe-Mitarai, T. Hara, S. Miura, H. Hosoda, Intermetallics 18 (2010) 2275–2280.
[6] Y. Xu, K. Otsuka, E. Furubayashi, T. Ueki, K. Mitsoe, Mater. Lett. 30 (1997) 189–197.
[7] X.L. Meng, W. Cai, Y.F. Zheng, Y.X. Tong, L.C. Zhao, L.M. Zhou, Mater. Lett. 55 (2002) 111–115.
[8] K. Otsuka, K. Oda, Y. Ueno, M. Piao, T. Ueki, H. Horikawa, Scripta Metall. Mater. 29 (1993) 1355–1358.
[9] S. Shimizu, Y. Xu, E. Okunishi, S. Tanaka, K. Otsuka, K. Mitose, Mater. Lett. 34 (1998) 23–29.
[10] R. Delville, D. Schryvers, Intermetallics 18 (2010) 2353–2360.
[11] M. Nishida, T. Hara, M. Matsuda, S. Ii, Mater. Sci. Eng. A 481–482 (2008) 18–27.
[12] T. Yamamuro, Y. Morizono, J. Honjyo, M. Nishida, Mater. Sci. Eng. A 438–440 (2006) 327–331.
[13] A. Kulińska, P. Wodniecki, Intermetallics 15 (2007) 1190–1196.
[14] K. Mizuuchi, K. Inoue, K. Hamada, K. Yamauchi, K. Enami, M. Sugioka, M. Itami, Y. Okanda, Mater. Sci. Eng. A 329–331 (2002) 557–562.
[15] C. Declairieux, A. Denquin, P. Ochin, R. Portier, P. Vermaut, Intermetallics (2011), doi:10.1016/j.intermet.2011.05.028.
[16] S. Besseghini, F. Passaretti, E. Villa, P. Fabbro, F. Ricciardi, Gold Bull. 40 (4) (2007) 328–335.
[17] S. Wu, C. Wayman, Metallography 20 (3) (1987) 359–376.
[18] H. Hosoda, R. Tachi, T. Inamura, K. Wakashima, S. Miyazaki, Mater. Sci. Forum 561–565 (2007) 1541–1544.
[19] H. Donkersloot, J.H.N Van Vucht, J. Less-Common Met. 20 (2) (1970) 83–91.
[20] M.S. El-Eskandarany, K. Aoki, K. Suzuki, J. Less-Common Met. 167 (1) (1990) 113–118.
[21] J. Eckert, L. Schultz, K. Urban, Appl. Phys. Lett. 55 (2) (1989) 117–119.
[22] M.S. El-Eskandarany, J. Alloys Compd. 279 (2) (1998) 263–271.
[23] S.L. Zhu, X.J. Yang, D.H. Fu, L.Y. Zhang, C.Y. Li, Z.D. Cui, Mater. Sci. Eng. A 408 (2005) 264–268.
[24] G.E. Monastyrsky, V. Odnosum, J. Van Humbeeck, V.I. Kolomytsev, Y.N. Koval, Intermetallics 10 (2002) 95–103.
[25] C.W. Goh, Y.W. Gu, C.S. Lim, B.Y. Tay, Intermetallics 15 (2007) 461–467.
[26] T. Yamamoto, H. Kato, Y. Murakami, H. Kimura, A. Inoue, Acta Mater. 56 (2008) 5927–5937.
[27] B. Yuan, C.Y. Chung, P. Huang, M. Zhu, Mater. Sci. Eng. A 438-440 (2006) 657–660.
[28] M. Igharo, J.V. Wood, Powder Metall. 28 (1985) 131.
[29] A. Biswas, Acta Mater. 53 (2005) 1415–1425.
[30] H.C. Yi, J.J. Moore, Scripta Metall. 22 (1998) 1889.

[31] L. Krone, E. Schüller, M. Bram, H.P. Buchkremer, D. Stover, Mater. Sci. Eng. A 378 (2004) 185.
[32] A.M. Locci, R. Orru, G. Cao, Z.A. Munir, Intermetallics 11 (2003) 555.
[33] B. Bertheville, J.H. Biaux, Scripta Metall. 52 (2005) 507.
[34] B. Bertheville, J.H. Biaux, J. Alloys Compd. 387 (2005) 211.
[35] Y. Suzuki, H. Unuma, Method for the preparation of an alloy of nickel and titanium (1998) US Patent 4,719,077.
[36] J. Mentz, M. Bram, H.P. Buchkremer, S. Stöver, Adv. Eng. Mater. 8 (4) (2006) 247–252.
[37] J. Mentz, M. Bram, H.P. Buchkremer, S. Stöver, Mater. Sci. Eng. A 481–482 (2008) 630–634.
[38] H.X. Zheng, J. Mentz, M. Bram, H.P. Buchkremer, D. Stöver, J. Alloys Compd. 463 (1–2) (2008) 250–256.
[39] A.R. Abbasi, M. Shamanian, J. Alloys Compd. 509 (31) (2011) 8097–8104.
[40] A.R. Abbasi, M. Shamanian, Mater. Sci. Eng. A 528 (9) (2011) 3295–3301.
[41] B. Tian, Y.X. Tong, F. Chen, Y. Liu, Y.F. Zheng, J. Alloys Compd. 477 (2009) 576–579.
[42] B. Tian, F. Chen, Y.X. Tong, L. Li, Y.F. Zheng, Y. Liu, Q.Z. Li, J. Alloys Compd. 509 (13) (2011) 4563–4568.
[43] M. Valeanu, M. Lucaci, A.D. Crisan, M. Sofronie, L. Leonat, V. Kuncser, J. Alloys Compd. 509 (13) (2011) 4495–4498.
[44] G.K. Williamson, W.H. Hall, Acta Metall. 1 (1) (1953) 22–31.
[45] ICSD Database FIZ Karlsruhe 2009-02, version 2.3.
[46] M.J. Phasha, A.S. Bolokang, P.E. Ngoepe, Mater. Lett. 64 (10) (2010) 1215–1218.
[47] W. Hume-Rothery, Acta Metall. 14 (1) (1966) 560–562.
[48] PowderCell for Windows Version 2.4, W. Kraus, G., Nolze, Federal Institute for Materials Research and Testing Rudower Chanssee 5, 12489, Berlin, Germany.